Mesoscopic Rough Electrical Double Layers

Weiqiang Tang,[1,*,†] Jinwen Liu,[2,*] Katharina Doblhoff-Dier,[2,‡] and Jun Huang[1,3,§]
[1]Institute of Energy Technologies, IET-3: Theory and Computation of Energy Materials, Forschungszentrum Jülich GmbH, 52425 Jülich, Germany
[2]Leiden Institute of Chemistry, Leiden University, Leiden 2300 RA, The Netherlands
[3]Faculty of Georesources and Materials Engineering, RWTH Aachen University, Aachen 52062, Germany

(Received 31 July 2025; accepted 22 December 2025; published 21 January 2026)

Fundamental understanding of electrical double layers (EDL) has been gleaned mostly on ideally planar electrodes, while realistic electrodes usually exhibit surface roughness on multiple scales. The influence of mesoscopic roughness (1–10 nm) is elusive, representing a cutting-edge challenge to theoretical modeling as both quantum- and classical-mechanical effects should be treated efficiently on the same footing. Addressing this challenge, we combine semiclassical models and Kohn-Sham density functional theory calculations to study the influence of mesoscopic roughness on the work function and the potential of zero free charge (PZFC) of silver electrodes. While the work function decreases at rougher electrodes as expected, the change in the PZFC is, unexpectedly, much smaller. The weakened correlation between work function and PZFC is ascribed to the decreased interfacial permittivity in the valley caused by a large, local, electron-spilling-induced electric field. In addition, the rough EDL at PZFC is heterogeneously charged with excess cations in the valley and excess anions near the peak, leading to the deviation of the potential of minimal capacitance from the PZFC.

DOI: 10.1103/bwdx-3yf3

Introduction—Surface roughness of metal-solution interfaces is ubiquitous in electrochemical systems [1,2], nanofluidics [3], and plasmonic systems [4,5]. Surface roughness includes steps, kinks, defects, dendrites, nanograins, pits, and fractures, spanning from atomistic, to nanometric, and to macroscopic scales [6,7]. Surface roughness affects both activity and selectivity of electrochemical reactions taking place at the interface [8–13]. In our perspective, an adequate understanding of the impact of surface roughness on electrochemical reactions needs to include a fundamental understanding of electrical double layer (EDL) forming at rough surfaces. There has been unattenuated interest in understanding the impact of surface roughness on fundamental properties of EDLs, including the work function, [14] the potential of zero free charge (PZFC) [15–18], and the double layer capacitance [19–24]. Previous works can be broadly divided into three groups, as illustrated in Fig. 1. The first group focuses on atomistic roughness, including steps, kinks, and defects [25,26], the second focuses on mesoscopic roughness on the scale of Debye length—the characteristic length of EDL [19,21,27,28], and the third focuses on macroscopic roughness on the scale of diffusion length [29–31].

At different scales, different factors dominate interfacial properties. Short-range, quantum mechanical, electronic factors dominate on the atomistic scale. These can be accurately addressed by Kohn-Sham density functional theory (DFT) calculation [17,24]. Classical mass transport dominates roughness effects observed on the macroscopic scale. On the mesoscale, both short-range, quantum-mechanical, electronic effects and long-range, classical, electrostatic effects are important. Previous works, however, have focused mainly on latter aspects [19–21,23,32]. For instance, Goldstein *et al.* [32] developed a perturbation approach to treat weak, mesoscopic roughness using Poisson-Boltzmann equations. Using the perturbation approach, Daikhin *et al.* [19,21] derived analytical expressions describing the influence of mesoscopic roughness on the double layer capacitance. Beyond these perturbative treatments, Poisson-Boltzmann-based mean-field models have also been extended to confined geometries such as nanoporous electrodes. Kondrat and Kornyshev [33,34] demonstrated that image-force-induced exponential screening enables dense ion packing in metallic nanopores, giving rise to very high capacitance when the pore size approaches

*These authors contributed equally to this work.
†Present address: Interdisciplinary Research Center for Sustainable Energy Science and Engineering (IRC4SE^2), School of Chemical Engineering, Zhengzhou University, Zhengzhou 450001, China.
‡Contact author: k.doblhoff-dier@lic.leidenuniv.nl
§Contact author: ju.huang@fz-juelich.de

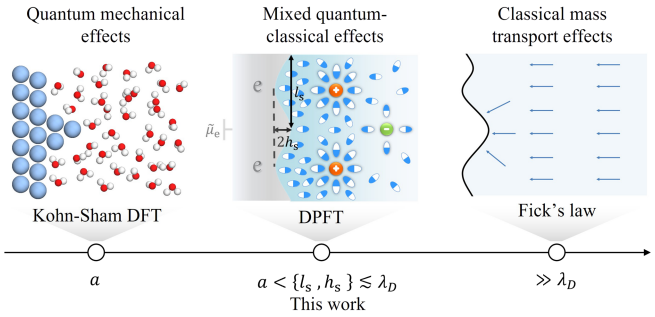

FIG. 1. The scale spectrum of studies on surface roughness. The surface roughness can be broadly divided into three scales: atomistic, mesoscopic, and macroscopic roughness. On the atomistic scale, short-range geometric and electronic factors dominate, which can be addressed adequately by Kohn-Sham density functional theory calculations. On the macroscopic scale, mass transport described using Fick's law is the dominant factor. This work focuses on mesoscopic roughness, where short-range electronic and long-range electrostatic effects are equally important and addressed using density-potential functional theoretical method under constant electrochemical potential of electrons $\tilde{\mu}_e$. Specifically, we consider a sinusoidal surface with two characteristic lengths, i.e., the roughness length l_s and the roughness height h_s. a and λ_D are the lattice constant of the metal and Debye length, respectively.

the ion diameter. These classical models focus solely on the electrolyte part of the EDL while treating the metal part as a featureless boundary. Hence, they fall short in capturing the interplay between metal electronic effects and classical electrostatic interactions in the presence of mesoscopic roughness. This is the gap that this work aims to fill. In principle, molecular dynamics (MD) simulations, including both DFT-based MD and classical MD (when coupled to the Siepmann-Sprik model [35]), can be used to bridge this gap and to explore rough and defective electrochemical interfaces. Cheng and co-workers, for example, employed DFT-based MD to study stepped metal-water interfaces, revealing the role of step density in modulating water chemisorption and the PZFC [17]. More recently, they developed a machine learning potential for the Pt(211)-water interface and performed large-scale simulations that uncovered anisotropic interfacial water structures and hydrogen-bond dynamics [36]. MD studies from the groups of Salanne [37,38] and Bocquet [39] have further elucidated ion and solvent structure near defective and nanostructured electrodes. These molecular-level simulations provide valuable insights into structural and dynamic heterogeneity at electrochemical interfaces, thereby complementing continuum and semiclassical theories. Importantly, molecular-level studies have shown that surface morphology not only alters ionic distributions but also reshapes the interfacial water structure hydrogen-bond network [17,40], and adsorption behavior [41,42], with direct consequences for solvation free energy, adsorption thermodynamics, and the electronic properties of the EDL. Nevertheless, their computational cost and the difficulty to simulate EDLs under constant potential conditions limit direct application to mesoscale systems [43].

A viable alternative is the recently developed density-potential functional theoretical (DPFT) method. Inspired by earlier jellium models of EDL [44,45], DPFT models combine an orbital-free quantum mechanical description of delocalized electrons in the metal and a classical statistical field description of the electrolyte solution [46–49]. Without enumerating Kohn-Sham orbitals, DPFT provides a computationally efficient method to simulate EDLs on the mesoscale. Importantly, in DPFT, the electrostatic potential is an explicit variable of equal status as the electron density, in sharp contrast with Kohn-Sham DFT where electron density and electrostatic potential are dual variables. DPFT thus allows us to explicitly control the inner potential of the metal phase, equivalent to controlling the electrode potential [50]. The advantages offered by orbital-free DFT come, however, at a price. DPFT itself cannot treat chemisorption, unless coupled with the model Hamiltonian of chemisorption as in Ref. [47]. Furthermore, DPFT neglects the atomistic structure of the electrolyte solution. Being aware of the shortcomings, we consider ideally polarizable EDLs without chemisorption in this work and employ Kohn-Sham DFT to check the DPFT results at affordable scales.

DPFT is validated and parametrized in two steps; see Supplemental Material note 1 [51]. In the first step, we compare the influence of atomistic roughness on the work function of a series of Ag-vacuum interfaces using DPFT and Kohn-Sham DFT. In the second step, we compare DPFT-based and experimental double layer capacitance curves of atomically flat Ag-aqueous solution interfaces, as measured by Valette [52]. Semiquantitative agreement is obtained in both steps (see note 1 [51]). We then employ the resulting, reasonably parametrized DPFT model to study the influence of mesoscopic roughness first on the work function, and then on the PZFC. Thereafter, the correlation between work function and PZFC at rough electrodes is interrogated using first DPFT and then *ab initio* molecular dynamics (AIMD) to test the DPFT-based insights.

The work function of Ag-vacuum interfaces with mesoscopic roughness—We now extend the DPFT model that has been verified for Ag-vacuum interfaces with atomic roughness (see note 1 [51]) to nanometric roughness. To do so, we simplify the model even further: Since an Ag nanosphere of 1.6 nm radius already contains over 1000 atoms, the discreteness of metal atoms can be further smoothened out and the mesoscopically rough metal is modeled as an electron gas situated against a positively charged background, namely, jellium. Specifically, we consider sinusoidal electrode surfaces, as depicted in Fig. 1, characterized by two parameters: the roughness

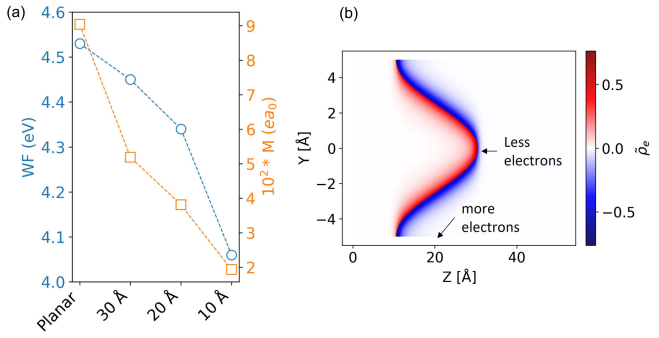

FIG. 2. Work functions of Ag-vacuum interfaces with mesoscopic sinusoidal roughness. (a) The work function and the moment of the electron density distribution M, as defined in Eq. (1), for sinusoidal Ag-vacuum interfaces. Here, we fix the roughness height $h_s = 10$ Å and vary l_s (larger values mean flatter surfaces). (b) Net electronic charge density normalized with respect to positive background charge density n_{cc}, $\tilde{\rho}_e = (n_{cc} - n_e)/n_{cc}$, for the case of $l_s = 10$ Å. Electron deficiency is found near the peak, and electron excess is found in the valley.

length l_s and the roughness height h_s. The values of l_s and h_s are between the lattice constant ($a \approx 4.08$ Å for Ag) and the Debye length ($\lambda_D \approx 30$ Å for 10 mM KPF_6 aqueous solution in this work).

The DPFT model reveals that work function decreases from 4.53 eV at an ideally planar surface to 4.06 eV at the rough surface with $l_s = 10$ Å, as shown in Fig. 2(a). That work function decreases with increasing surface roughness is thus a general trend for both atomistic roughness, as shown in Fig. S1 [51], and mesoscopic roughness. This decreasing trend is caused by the electronic charge density smoothening out atomic roughness, leading to an electronic dipole moment opposing that of the metal surface. At the atomic scale, this effect is known from previous studies as the Smoluchowski effect [53–55]. As illustrated in Fig. 2(b), valleys have excess electrons, whereas hills have excess deficit compared to the planar case. We quantify this countering effect by calculating the moment of the electron density distribution M as

$$M = ea_0 \frac{\iint (\bar{n}_e - \bar{n}_{cc}) \Delta\bar{z}\, d\bar{y} d\bar{z}}{\bar{l}_{real}}. \quad (1)$$

Here, $\bar{n}_e$ and $\bar{n}_{cc}$ represent the dimensionless electron density and charge density of metal cationic cores, both normalized to $n_{ref} = a_0^{-3}$ with a_0 the Bohr radius. $\Delta\bar{z}$ is the dimensionless horizontal distance of a point to the electrode surface edge. $\bar{l}_{real}$ is the real (i.e., nonprojected) length of the sinusoidal Ag surface in the unit cell normalized to a_0. M decreases from planar to rougher surfaces, as shown in Fig. 2(a). A smaller M results in a reduced potential drop at the metal surface, namely, a smaller surface potential. Provided that the chemical potential of electrons in the bulk metal is unchanged, a smaller surface potential results in a smaller work function.

PZFC of the Ag solution interfaces with mesoscopic roughness—To simulate double layer capacitance (C_{dl}) curves, we use the DPFT model parametrized using experimental C_{dl} curves of the Ag(111) electrode in aqueous solution of x mM KPF_6 ($x = 5$, 10, 20, 40, and 100) reported by Valette [52], see Supplemental Material note 1 [51]. We keep the parameters constant and simulate planar ($l_s = \infty$), and three rough Ag electrodes ($h_s = 10$ Å, $l_s = 30, 20, 10$ Å) in 10 mM KPF_6. Figure 3(a) shows a shift in the potential of minimal double layer capacitance (PMC) and a change in the magnitude of C_{dl}. In general, the PMC shifts negatively when the surface gets rougher. The magnitude of C_{dl} per projected surface area generally grows when the surface gets rougher ($l_s = \infty \to 30 \to 20$ Å). However, the increasing trend is reversed for the case of $l_s = 10$ Å at negative potentials, when valleys get too narrow to accommodate cations. The sharp increase of C_{dl} at $l_s = 10$ Å at more positive potentials (more positive $-\tilde{\mu}_e$) can be explained by anions with a smaller size than cations penetrating the valley.

Intriguingly, the electrochemical potential at which the net ionic charge in the electrolyte solution is zero, denoted $\tilde{\mu}_{e,PZFC}$, does not coincide with PMC for rough surfaces. This mismatch is in stark contrast to what is known for planar surfaces. The deviation occurs because the rough EDL is heterogeneous in that the valley is filled with excess cations while the peak region features excess anions, see Fig. 3(c), though the overall electrolyte solution is electroneutral at $\tilde{\mu}_{e,PZFC}$. Cation accumulation in the valley region is caused by excess electrons "spilling" into the valley as shown in Fig. 3(d). Similarly, anion accumulation near the peak is caused by an electron deficiency at the peaks. A similar scenario can be found in polycrystalline electrodes [18,56] and in overlapping EDLs at supported nanoparticles [57].

We calculate the absolute PZFC as $E^{abs}_{PZFC} = -\tilde{\mu}_{e,PZFC}/e_0$ [dashed lines in Fig. 3(a)], and plot E^{abs}_{PZFC} against WF for the four examined surfaces in Fig. 3(b). For homogeneous surfaces, a linear relation with a slope equal to 1 has been established between WF and PZFC with a vertical shift attributed to interfacial water [58]. This relation is indicated in Fig. 3(b) by a dashed line. For the rough surfaces as simulated here, a linear regression gives, however, a much lower slope of ~0.12, suggesting a much weaker correlation between WF and PZFC at mesoscopically rough electrodes. This weakened correlation appears to be relatively robust against changes in the model parametrization. For example, the correlation pertains when only 1s electrons are considered or when the gradient coefficient in the kinetic energy functional is changed, see Supplemental Material note 2 [51].

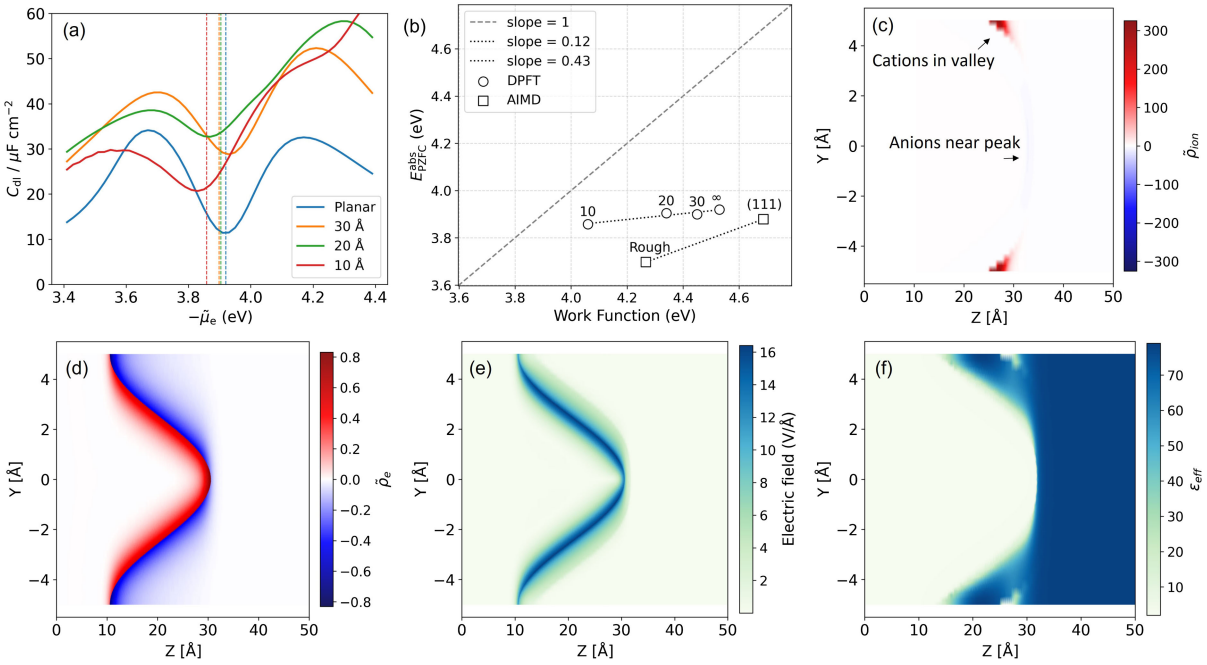

FIG. 3. Sinusoidal Ag-solution interfaces. (a) Double layer capacitance C_{dl} curves for planar ($l_s = \infty$) and three rough Ag electrodes ($h_s = 10$ Å, $l_s = 30, 20, 10$ Å) in 10 mM KPF_6. Model parameters are calibrated using experimental C_{dl} curves of Ag(111) electrode in aqueous solution of x mM KPF_6 ($x = 5, 10, 20, 40$ and 100) reported by Valette, [52] see Supplemental Material note 1 [51]. The dashed lines locate the values of $\tilde{\mu}_e$ with overall zero free charge in the EDL, denoted $\tilde{\mu}_{e,PZFC}$. It is noted that $\tilde{\mu}_{e,PZFC}$ and the potentials of minimal capacitance do not coincide, except for the ideally planar surface. (b) The relation between absolute potential of zero free charge, $E^{abs}_{PZFC} = -\tilde{\mu}_{e,PZFC}/e_0$, and work function for the four examined electrodes. The dashed line represents a linear relation with a unity slope, while the dotted line represents a linear regression. Squares correspond to AIMD simulations. (c) Dimensionless net ionic charge density, $\tilde{\rho}_{ion} = (n_c - n_a)/n^b_{ion}$, with n_c, n_a, and n^b_{ion} being cation, anion, bulk ion concentrations, respectively, for the rough electrode ($h_s = 10$ Å, $l_s = 10$ Å) at its $\tilde{\mu}_{e,PZFC}$. (d) Dimensionless net electronic charge density, $\tilde{\rho}_e = (n_{cc} - n_e)/n_{cc}$, with n_{cc} and n_e being cationic charge and electron densities, respectively, for the rough electrode ($h_s = 10$ Å, $l_s = 10$ Å) at its $\tilde{\mu}_{e,PZFC}$. (e) Electric field and (f) effective permittivity for the rough electrode ($h_s = 10$ Å, $l_s = 10$ Å) at its $\tilde{\mu}_{e,PZFC}$.

Origin of the weaker correlation between PZC and work function—Following our previous study on the solvent-dependency of PZFC of planar Au(111) electrodes [59], the much smaller change in PZFC compared to WF at rough surfaces can be expected to be associated with the interfacial permittivity distribution. It has been revealed that a lower permittivity near the electrode surface increases the potential drop at the interface at a given electron density distribution, and hence a more positive PZFC is obtained. Therefore, we hypothesize that a smaller local permittivity offsets the large decrease in the WF, resulting in a smaller decrease in PZFC at increasingly rough electrodes.

The relative permittivity distribution at the sinusoidal Ag-solution interface ($l_s = h_s = 10$ Å) is depicted in Fig. 3(f). We find that the permittivity is indeed much smaller in the valley due to two factors. On one hand, the large electric field near the metal surface, as shown in Fig. 3(e), reduces the screening capability of water dipoles in response to free charges [60,61]. On the other hand, the cation accumulation in the valley decreases the density of water molecules. The two combined effects on the local permittivity can be explained via

$$\epsilon_{eff} = \epsilon_{hf} + \kappa \bar{n}_s \bar{p}^2 \left[\coth(\bar{p}\,\bar{E}) - \frac{1}{\bar{p}\,\bar{E}} \right], \tag{2}$$

where ϵ_{hf} is the high-frequency component of permittivity, $\kappa = (e_0^2/k_B T \epsilon_0 a_0)$ is a fundamental constant resulting from nondimensionalization, $\bar{p} = (p/e_0 a_0)$ is the dimensionless dipole moment of water, $\bar{n}_s$ is the dimensionless water density, and $\bar{E} = |\nabla \bar{\phi}|$ is the dimensionless electric field. Equation (2) indicates that ϵ_{eff} is smaller at higher $\bar{E}$ and lower $\bar{n}_s$ suggesting that this could, indeed be the cause for the reduced slope observed for PZFC vs WF for rough surfaces.

For comparison, earlier theoretical frameworks such as the Bazant-Storey-Kornyshev (BSK) model [62] and the Brown hydration model [63] treated dielectric and solvation effects in different ways. The BSK model accounts for electrostatic correlations and finite ion size in solvent-free ionic liquids by introducing a nonlocal permittivity characterized by a correlation length, whereas the Brown model introduces short-range hydration forces as an external potential to explain the emergence of the Stern layer. In contrast, the present semiclassical DPFT formulation

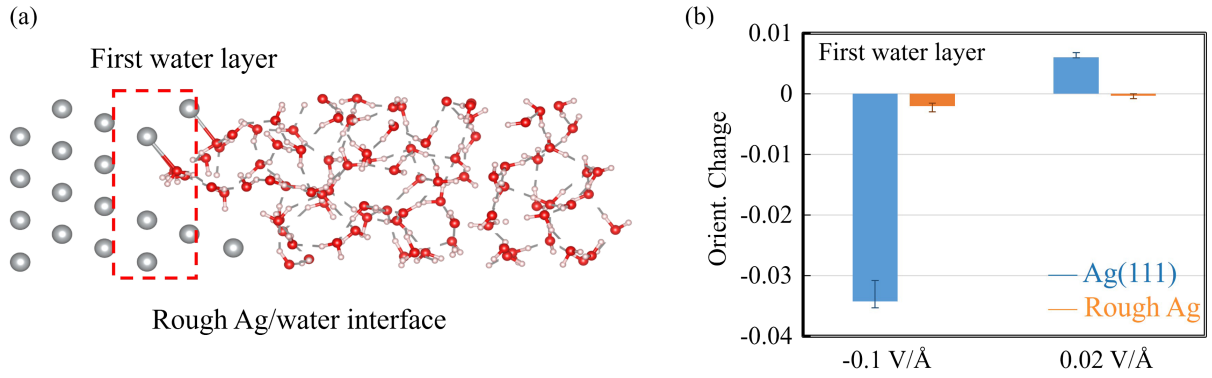

FIG. 4. (a) A representative snapshot during an AIMD simulation for the rough Ag-water interface. The first water layer region is highlighted in the red dotted box. (b) Orientation changes in the first water layer region for Ag(111)-water and rough Ag-water interfaces under −0.1 and 0.02 V/Å electric field.

describes the solvent response through a local, field- and density-dependent permittivity, which naturally reflects the combined effects of interfacial electric fields and solvent depletion near rough surfaces without invoking empirical potentials.

Verifying the weaker correlation between PZC and work function using AIMD—Since the DPFT model relies on parametrization, neglects the atomistic structure of the electrolyte, and disregards chemical interactions between water and Ag atoms, we performed AIMD simulations on nanoscopically rough Ag-water and Ag(111)-water interfaces. This allows us to test whether the deviating trend obtained between PZFC and WF in DPFT is real.

A representative snapshot for the rough Ag-water interface obtained in the AIMD simulations is shown in Fig. 4(a). Details of AIMD simulation and the analysis of interfacial water structure and the H-bonding network are provided in Supplemental Material note 3 [51]. From the simulations, we can obtain both the WF and the PZFC. Similarly to the DPFT results, we find the change in PZFC when going from atomically flat to a rough surface to be smaller than the change in the WF. This is also shown in Fig. 3(b). Although there are quantitative differences (with AIMD suggesting a slope of 0.43 and DPFT a slope of 0.12), the general trend of changes in the PZFC being smaller than changes in the WF remains.

To further understand the reduced PZFC-WF slope and test the hypothesis proposed earlier, we study the orientational change of the first-layer water molecules in response to applied electric fields in AIMD simulation and compare it with the DPFT predictions. Two field directions are considered: toward the bulk solution (defined as positive) and toward the metal bulk (defined as negative). To prevent bulk water molecules from migrating into the vacuum region (Fig. S9 [51]), a lower electric field magnitude (0.02 V/Å) was applied in the positive direction compared to the negative direction (−0.1 V/Å). As shown in Figs. S7 and S10 [51], the water density profiles under these electric fields exhibit negligible changes compared to the zero-charge case for both Ag(111) and rough Ag electrodes. Instead, the applied electric field primarily affects water molecules' orientation, as illustrated by the $\cos\varphi$ and $\Delta\cos\varphi$ distribution profiles in Figs. S13–S14 [51]. A positive field promotes an H-up configuration ($\cos\varphi > 0$), whereas a negative field favors an H-down configuration ($\cos\varphi < 0$).

To further analyze the reaction of the water molecules to the electric field, we analyzed the accumulated average water orientation change, defined as the integral of water dipole variations under an electric field vs no electric field, normalized by the integral of water density (Fig. S15 [51]). Figure 4(b) summarizes the changes in water orientation within the first interfacial layer under both positive and negative applied electric fields. On Ag (111), water molecules at the interface exhibit significant orientational changes in response to the applied field, which gradually stabilize in the bulk region. Both the interfacial response and the converged bulk values align with the direction of the applied field. In contrast, the first water layer near the rough Ag electrode undergoes significantly smaller orientational changes, tentatively indicating reduced polarizability and permittivity, consistent with the analysis based on the DPFT model. Although the reduced H bonding in the trough (see Fig. S16 [51]) would indicate an increased permittivity, a reduced reorientation could arise from a strong water-surface interaction within surface troughs. This finding aligns with experimental evidence showing that confined water possesses lower permittivity [61]. The reduced reorientation may, however, also be a consequence of the local electric field in the valleys being small due to tip enhancement of the electric field at the rough surface. Unfortunately, the local electric field cannot be derived from the Hartree potential obtained in the DFT calculations. (The Hartree potential includes the potential within the atoms and molecules, which is irrelevant to the water reorientation.) This highlights the relevance of simplified models such as DPFT to providing insight into the underlying physical processes.

Conclusions—We investigated the effects of mesoscopic roughness on work function and PZFC of silver electrodes in nonadsorbing aqueous electrolyte solutions. The WF of metal-vacuum interfaces decreases with increasing roughness, due to the Smoluchowski effect that describes spilling of electrons from the tips to the valleys of the rough surface. In contrast with noticeable WF changes when increasing the roughness, the changes in the PZFC are much smaller, deviating from the linear relation between WF and PZFC with a slope of unity established in the literature. This trend is confirmed in AIMD simulations. Based on our semiclassical model, we attribute the much weaker correlation between WF and PZFC to the permittivity decrement in the valley at mesoscopically rough Ag electrodes. In addition, we found that the potential of minimal capacitance does not coincide with the PZFC at mesoscopic rough electrodes. The mismatch is related to the charging heterogeneity of the rough EDL with excess cations in the valley and excess anions near the peak at the PZFC. Taken together, the results indicate that the semiclassical DPFT method with a unified treatment of mixed quantum and classical mechanical effects is a viable theoretical approach to model EDLs with mesoscopic roughness.

Acknowledgments—This work received funding from the Initiative and Networking Fund of the Helmholtz Association (No. VH-NG-1709) and the European Research Council (ERC) (starting Grant No. 101163405 "MESO-CAT," and advanced Grant No. 101019998 "FRUMKIN"). This publication is part of the project "Computational Electrochemistry" with file No. 2025.014 of the research program "Computing Time on National Computer Facilities" which is (partly) financed by the Dutch Research Council (NWO).

Views and opinions expressed are, however, those of the authors only and do not necessarily reflect those of the European Union or the European Research Council. Neither the European Union nor the granting authority can be held responsible for them.

Data availability—The data supporting the findings of this article are openly available [64], embargo periods may apply.

[1] L. Jacobse, Y.-F. Huang, M. T. M. Koper, and M. J. Rost, Nat. Mater. **17**, 277 (2018).
[2] R. Amirbeigiarab, J. Tian, A. Herzog, C. Qiu, A. Bergmann, B. Roldan Cuenya, and O. M. Magnussen, Nat. Catal. **6**, 837 (2023).
[3] R. Qiao, Microfluid. Nanofluid. **3**, 33 (2007).
[4] C. Ciracì, F. Vidal-Codina, D. Yoo, J. Peraire, S.-H. Oh, and D. R. Smith, ACS Photonics **7**, 908 (2020).
[5] S. Ding, L. Ma, J. Feng, Y. Chen, D. Yang, and Q. Wang, Nano Res. **15**, 2715 (2022).
[6] R. G. Mariano, K. McKelvey, H. S. White, and M. W. Kanan, Science **358**, 1187 (2017).
[7] K. Oura, V. Lifshits, A. Saranin, A. Zotov, and M. Katayama, *Surface Science: An Introduction* (Springer Science & Business Media, 2013).
[8] Y. Jiang, D. Zhong, L. Wang, J. Li, G. Hao, J. Li, and Q. Zhao, Chem. Asian J. **17**, e202200380 (2022).
[9] K. Jiang, Y. Huang, G. Zeng, F. M. Toma, W. A. Goddard III, and A. T. Bell, ACS Energy Lett. **5**, 1206 (2020).
[10] C. L. Bentley, M. Kang, and P. R. Unwin, J. Am. Chem. Soc. **141**, 2179 (2019).
[11] Y. Yoon, A. S. Hall, and Y. Surendranath, Angew. Chem., Int. Ed. Engl. **55**, 15282 (2016).
[12] D. Cheng, K. L. C. Nguyen, V. Sumaria *et al.* Nat. Commun., **16**, 4064 (2025)..
[13] K.-L. C. Nguyen, J. P. Bruce, A. Yoon, J. J. Navarro, F. Scholten, F. Landwehr, C. Rettenmaier, M. Heyde, and B. R. Cuenya, ACS Energy Lett. **9**, 644 (2024).
[14] J. Kaur and R. Kant, J. Phys. Chem. C **121**, 13059 (2017).
[15] G. K. Mishra and R. Kant, J. Phys. Chem. C **125**, 25774 (2021).
[16] A. S. Shatla, M. Landstorfer, and H. Baltruschat, ChemElectroChem. **8**, 1817 (2021).
[17] A. Chen, J.-B. Le, Y. Kuang, and J. Cheng, J. Chem. Phys. **157**, 094702 (2022).
[18] N. L. Fröhlich, J. Liu, K. Ojha, A. Hagopian, K. Doblhoff-Dier, and M. T. M. Koper (to be published).
[19] L. I. Daikhin, A. A. Kornyshev, and M. Urbakh, Phys. Rev. E **53**, 6192 (1996).
[20] L. Daikhin, A. Kornyshev, and M. Urbakh, Electrochim. Acta **42**, 2853 (1997).
[21] L. Daikhin, A. Kornyshev, and M. Urbakh, J. Chem. Phys. **108**, 1715 (1998).
[22] T. Aslyamov, Curr. Opin. Electrochem. **35**, 101104 (2022).
[23] T. Aslyamov, K. Sinkov, and I. Akhatov, Phys. Rev. E **103**, L060102 (2021).
[24] S. Xue, P. Chaudhary, M. R. Nouri, E. Gubanova, B. Garlyyev, V. Alexandrov, and A. S. Bandarenka, J. Am. Chem. Soc. **146**, 3883 (2024).
[25] B. Hagman, A. Posada-Borbón, A. Schaefer, M. Shipilin, C. Zhang, L. R. Merte, A. Hellman, E. Lundgren, H. Grönbeck, and J. Gustafson, J. Am. Chem. Soc. **140**, 12974 (2018).
[26] K. J. P. Schouten, E. P. Gallent, and M. T. M. Koper, J. Electroanal. Chem. **699**, 6 (2013).
[27] J. Wei, Y. Li, D. Dai, F. Zhang, H. Zou, X. Yang, Y. Ji, B. Li, and X. Wei, ACS Appl. Mater. Interfaces **12**, 5786 (2020).
[28] G. Palasantzas and G. M. E. A. Backx, Phys. Rev. E **69**, 041603 (2004).
[29] H. Li *et al.*, Mater. Horiz. **9**, 1788 (2022).
[30] Y. Liu, H. Jiang, and Z. Hou, Angew. Chem. **133**, 11233 (2021).
[31] Y. E. Seidel, A. Schneider, Z. Jusys, B. Wickman, B. Kasemo, and R. J. Behm, Faraday Discuss. **140**, 167 (2009).
[32] R. E. Goldstein, A. I. Pesci, and V. Romero-Rochn, Phys. Rev. A **41**, 5504 (1990).
[33] S. Kondrat and A. Kornyshev, J. Phys. Condens. Matter **23**, 022201 (2010).
[34] S. Kondrat, C. R. Pérez, V. Presser, Y. Gogotsi, and A. A. Kornyshev, Energy Environ. Sci. **5**, 6474 (2012).

[35] J. I. Siepmann and M. Sprik, J. Chem. Phys. **102**, 511 (1995).
[36] F.-T. Wang, X. Liu, and J. Cheng, Mater. Futures **3**, 041001 (2024).
[37] C. Merlet, C. Péan, B. Rotenberg, P. A. Madden, B. Daffos, P. L. Taberna, P. Simon, and M. Salanne, Nat. Commun. **4**, 2701 (2013).
[38] K. G. Reeves, D. Dambournet, C. Laberty-Robert, R. Vuilleumier, and M. Salanne, RSC Adv. **10**, 8982 (2020).
[39] L. Scalfi, M. R. Becker, R. R. Netz, and M.-L. Bocquet, Commun. Chem. **6**, 236 (2023).
[40] P. Li, Y. Liu, and S. Chen, J. Chem. Phys. **156**, 104701 (2022).
[41] B. Hammer and J. K. Nørskov, in *Advances in Catalysis* (Academic Press, New York, 2000), p. 71.
[42] I. T. McCrum and M. J. Janik, ChemElectroChem **3**, 1609 (2016).
[43] A. Groß, in *Surface and Interface Science*, edited by K. Wandelt (Wiley, New York, 2020), p. 471.
[44] J. P. Badiali, M. L. Rosinberg, and J. Goodisman, J. Electroanal. Chem. Interfacial Electrochem. **143**, 73 (1983).
[45] W. Schmickler, J. Electroanal. Chem. Interfacial Electrochem. **150**, 19 (1983).
[46] J. Huang, P. Li, and S. Chen, Phys. Rev. B **101**, 125422 (2020).
[47] J. Huang, S. Chen, and M. Eikerling, J. Chem. Theory Comput. **17**, 2417 (2021).
[48] J. Huang, Electrochim. Acta **389**, 138720 (2021).
[49] J. Huang, J. Chem. Theory Comput. **19**, 1003 (2023).
[50] M. M. Melander, T. Wu, T. Weckman, and K. Honkala, npj Comput. Mater. **10**, 5 (2024).
[51] See Supplemental Material at http://link.aps.org/supplemental/10.1103/bwdx-3yf3 for technical details of DPFT, Kohn-Sham DFT, AIMD calculations, and additional results and discussions.
[52] G. Valette, J. Electroanal. Chem. Interfacial Electrochem. **269**, 191 (1989).
[53] R. Smoluchowski, Phys. Rev. **60**, 661 (1941).
[54] J. Hölzl, F. K. Schulte, and H. Wagner, *Solid Surface Physics* (Springer, New York, 2006), Vol. 85.
[55] W. Li and D. Li, J. Chem. Phys. **122**, 064708 (2005).
[56] H. Ibach, G. Beltramo, and M. Giesen, Surf. Sci. **605**, 240 (2011).
[57] Y. Zhang, T. Binninger, J. Huang, and M. H. Eikerling, Phys. Rev. Lett. **134**, 066201 (2025).
[58] S. Trasatti, J. Electroanal. Chem. Interfacial Electrochem. **33**, 351 (1971).
[59] W. Tang, S. Zhao, and J. Huang, JACS Au **3**, 3381 (2023).
[60] F. Deißenbeck, C. Freysoldt, M. Todorova, J. Neugebauer, and S. Wippermann, Phys. Rev. Lett. **126**, 136803 (2021).
[61] L. Fumagalli *et al.*, Science **360**, 1339 (2018).
[62] M. Z. Bazant, B. D. Storey, and A. A. Kornyshev, Phys. Rev. Lett. **106**, 046102 (2011).
[63] M. A. Brown, G. V. Bossa, and S. May, Langmuir **31**, 11477 (2015).
[64] 10.5281/zenodo.18020211.